14A.7 SEA SURFACE TEMPERATURE BIASES UNDER THE STRATUS CLOUD DECK IN THE SOUTHEAST PACIFIC OCEAN IN 19 IPCC AR4 COUPLED GENERAL CIRCULATION MODELS

Yangxing Zheng[1*], Toshiaki Shinoda[2], Jia-Lin Lin[3], George N. Kiladis[4]
[1]*CIRES, University of Colorado, Boulder, Colorado*
[2]*Naval Research Laboratory, Stennis Space Center, Mississippi*
[3]*Department of Geography, The Ohio State University, Columbus, Ohio*
[4]*NOAA/ESRL Physical Science Division, Boulder, Colorado*

1. Introduction

Climate in the southeast Pacific (SEP) near the coast of Peru and Chile is controlled by complex upper-ocean, marine boundary layer and land processes and their interactions. A variety of coupled processes between ocean and atmosphere are involved in this tightly coupled system, and the variation of the system has significant impacts on global climate (e.g., Ma et al. 1996; Miller 1997; Gordon et al. 2000; Xie 2004). For example, strong winds parallel to the coast generate intense coastal upwelling, bringing cold water to the ocean surface, which helps to maintain the persistent stratus/stratocumulus cloud decks by stabilizing lower troposphere. These persistent stratus cloud decks have a substantial impact on surface energy budget in the tropics and subtropics by reflecting sunlight back to space.

Unfortunately, coupled atmosphere-ocean general circulation models (CGCMs) have systematic errors in the SEP region, including a warm bias in SST and too little cloud cover (e.g. Mechoso et al. 1995; Ma et al. 1996; Gordon et al. 2000; McAvaney et al. 2001; Kiehl and Gent 2004; Large and Danabasoglu 2006; Wittenberg et al. 2006; Lin 2007). These biases have important impacts on the simulated earth's radiation budget and climate sensitivity. Also, the accurate prediction of low clouds over the SEP is required to simulate the strong trade winds and the observed SST distribution in the tropics (Ma et al. 1996; Gordon et al. 2000).

* *Corresponding author address*: Yangxing Zheng, CIRES, University of Colorado, Boulder, Colorado, 80305; email: Yangxing.Zheng@noaa.gov

Although previous studies described above reported a warm SST bias in the SEP region in some CGCMs, it is still uncertain whether a similar bias is evident in most state-of-the-art CGCMs and to what extent the SST biases are model dependent. Recently, in preparation for the Intergovernmental Panel on Climate Change (IPCC) Fourth Assessment Report (AR4), many international climate-modeling centers conducted a comprehensive set of climate simulation for the twentieth century's climate and different climate change scenarios in the twenty-first century. The release of the output of IPCC AR4 CGCMs simulations provided the opportunity to investigate the systematic biases in the SEP region using long-term simulations with a variety of CGCMs. In fact, de Szoeke and Xie (2008) found the warm SST error on the equator near the South American coast (2^oS-2^oN, 90^oW-80^oW) in IPCC AR4 CGCMs simulations and attributed the error to a weak meridional wind compared to observations. In this study, we will quantify systematic SST biases in the SEP region in these IPCC AR4 CGCMs simulations, and attempt to isolate their causes.

Since the SEP climate is a tightly coupled system, inaccurate simulations of both atmospheric and oceanic processes and their interactions may contribute to the SST biases. Accordingly, it is necessary to examine individual biases in the OGCMs, and the AGCMs, along with the biases in the accompanying ocean-atmosphere feedback processes in order to provide useful guidance on how to improve the CGCM simulations. Importance of three-dimensional upper ocean processes for controlling SST in the SEP region has been recently demonstrated by observations, OGCM and CGCM experiments (Colbo and Weller 2007; Shinoda and Lin 2009; Zheng et al. 2010; Toniazzo et al. 2010). For example, Zheng et al. (2010) estimated the annual mean heat budget using eddy-resolving OGCM experiments, and indicated the dominant role of horizontal advection of upwelled cold water from the coast in balancing the positive surface heat flux and thus maintaining the annual mean SST in the SEP region. Hence the accurate simulation of upper ocean processes as well as air-sea fluxes is crucial for predicting SSTs in this region.

The deficiency in simulating upper ocean processes in the SEP region is found in some CGCM experiments. For example, Large and Danabasoglu (2006) examined largest and potentially most important ocean near-surface biases in the Community Climate version 3 (CCSM3) coupled simulation of present-day conditions. The largest mean SST biases develop along the eastern boundaries of subtropical gyres including the SEP region, and the overall coupled model response is found to be linear. Based on the subsequent ocean-only experiment, they suggested that the cause of the warm bias in the southeastern tropical oceans could be traced back to inadequate coastal upwelling close to the coast; that is, the cause was partially contained in the ocean model.

A major focus of the present study is to identify upper ocean processes and surface fluxes that could be relevant to SST biases in CGCMs. Although the data coverage of in-situ observations in the upper ocean and air-sea fluxes in the SEP region are still sparse, global data sets of surface fluxes (e.g., the Objectively Analyzed air-sea Heat Fluxes; Yu and Weller 2007) and ocean analysis (e.g., Simple Ocean Data Assimilation; Carton and Giese 2008) have been significantly improved in recent years because a variety of satellite data are included in the analyses. Hence it is now feasible to evaluate the CGCMs' ability to simulate air-sea fluxes and upper ocean currents and temperature. In this study, we will examine errors in upper ocean processes and surface fluxes in CGCMs that could contribute to the biases in SST. Major terms in the upper-ocean heat budget are estimated using the output of CGCMs, and they are compared with those from the ocean analysis and surface flux estimates based on satellite measurements.

2. Models and validation datasets

a. IPCC models

The analysis is based on 20-yr (1980-1999) model runs of the Climate of the Twentieth Century (20C3M) simulations from 19 coupled GCMs. Table 1 shows the model names and acronyms, their ocean model horizontal and vertical resolutions, heat flux corrections, and which run is employed for analysis. The resolution of the ocean models within the stratus region is also shown. For each model, we use 20 years of monthly mean ocean temperature, salinity, three-dimensional ocean currents, surface wind stress, sea level pressure, surface downward/upward shortwave/longwave radiation, surface latent heat flux, surface sensible heat flux, and near-surface meteorological variables (wind speed at 10 m, air temperature and air specific humidity at 2 m).

b. SODA

The SODA methodology, the ingested data, and the error covariance structure of both the model and the observations are described by Carton et al. (2000a, b), Carton and Giese (2008), and Zheng and Giese (2009). The ocean model is based on the Los Alamos implementation of the Parallel Ocean Program (POP) (Smith et al. 1992). The model resolution is on average 0.4^{o} (lon) X 0.25^{o} (lat) with 40 levels in the vertical. The model is forced with the European Centre for Medium-Range Weather Forecasts (ECMWF) ERA-40 daily atmospheric reanalysis winds (Simmons and Gibson 2002) for the 44-year period from 1958 to 2001.

The model is constrained by abundant observed temperature and salinity using a sequential assimilation algorithm, which is described by Carton et al. (2000a, b) and Carton and Giese (2008). Surface heat fluxes are computed from bulk formulae (Smith et al. 1992), with atmospheric variables from the NCEP/NCAR reanalysis (Kalnay et al. 1996). The NCEP/NCAR reanalysis information is used for the bulk formulae instead of the ERA-40 variables throughout the experiment to give continuity of surface forcing during periods for which the ERA-40 winds are not available. However, the details of surface heat flux boundary condition are relatively unimportant in influencing the solution, since near-surface temperature observations are used to update the mixed layer temperature. Vertical diffusion of momentum, heat, and salt is based on a non-local K-Profile parameterization (KPP, Large et al. 1994) and horizontal diffusion for subgrid-scale processes is based on a biharmonic mixing scheme.

Averages of model output variables (temperature, salinity, and velocity) are saved at 5-day intervals. These average fields are remapped onto a uniform global 0.5^{o} X 0.5^{o} horizontal grid using the *horizontal grid spherical coordinate remapping and interpolation package* with second-order conservative remapping (Jones 1999).

c. Heat flux datasets

In this study, monthly mean surface fluxes from OAFlux (Yu and Weller 2007, Yu et al. 2008) are primarily used for evaluating the biases of heat fluxes in CGCMs, since they are the latest, and perhaps the best validated datasets. Near surface meteorological variables and SST used to estimate the fluxes are obtained from an optimal blending of satellite retrievals and two versions of NCEP reanalyses (i.e., NCEP1, NCEP2), and ERA-40. NCEP1 represents the NCEP/NCAR reanalysis project that has produced an ongoing dataset from 1948 to the present (Kalnay et al. 1996), and NCEP2 represents the NCEP/DOE reanalysis project in an effort to correct known errors in NCEP1 from 1979 to the present and to improve parameterizations of some physical processes (Kanamitsu et al. 2002). The latent and sensible fluxes are computed from the optimally estimated near surface atmospheric variables and SST using the Tropical Ocean Global Atmosphere Coupled Ocean-Atmosphere Response Experiment (TOGA COARE) bulk air-sea flux algorithm version 3.0 (Fairall et al. 2003). Surface latent and sensible heat fluxes as well as meteorological variables near the surface are available from January 1958-December 2008. Surface shortwave and longwave radiation of OAFlux is derived from the International Satellite Cloud Climatology Project (ISCCP)-FD estimates (Zhang et al. 2004) that are available from 1 July 1983. These flux estimates are compared to 107 (105 buoys and 2 ships) in-situ flux time series, and it is found that they are relatively unbiased and have the smallest mean error compared to other datasets (Yu and Weller 2007; Yu et al. 2008).

Since there are still significant uncertainties in surface heat flux estimates (e.g., Kubota et al. 2003; Brunke et al. 2003; Chou et al. 2004; Yu et al., 2007), we also use monthly mean heat fluxes from NCEP1, NCEP2, ERA-40, and the Goddard Satellite-Based Surface Turbulent Fluxes Version 2 (GSSTF2) for the evaluation of model surface fluxes. Latent and sensible heat fluxes in GSSTF2 are estimated from satellite-derived meteorological variables and SST with a bulk flux algorithm including salinity and cool-skin effects (Chou et al. 2003). Observational datasets and an ocean analysis dataset used for evaluating the model simulations are summarized in Table 2.

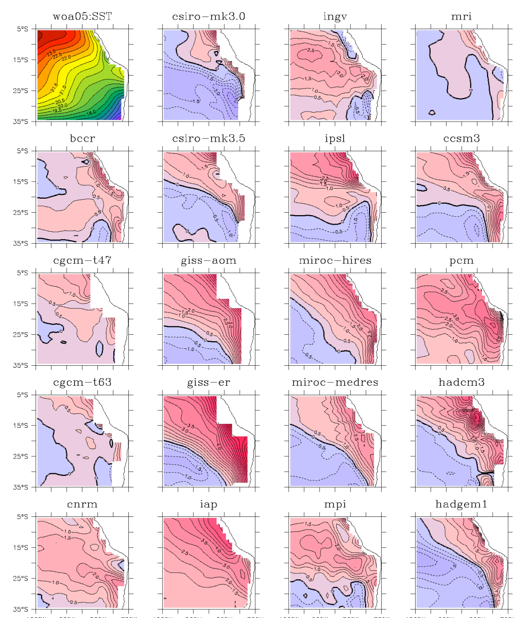

Figure 1. Top left panel: SST from World Ocean Atlas 2005 (WOA05). Other panels: Spatial distribution of the SST biases (shading contours in ^{o}C) relative to WOA05 from 19 IPCC AR4 coupled GCMs in the region (100^{o}W-70^{o}W, 35^{o}S-5^{o}S). Contour interval is 0.5^{o}C.

3. SST biases

Figure 1 shows the spatial distribution of SST biases in the southeast Pacific Ocean

(100°W-70°W, 35°S-5°S) from 19 IPCC AR4 coupled GCMs along with the mean SST averaged from World Ocean Atlas 2005 (WOA05) monthly climatology (Antonov et al. 2006; Locarniti et al. 2006) (shown in left top panel). The SST biases are computed as the difference between the model SST averaged over the period 1980 through 1999 and WOA05 SST. Warm biases in SST are evident in most models especially in northern part of stratus region, with the greatest values near the coast except in *ingv*, *mpi*. The warm SST biases are generally weaker in southern part of stratus region, and cold biases are found in some models. These latitudinal variations of SST biases are further shown in the SST biases averaged along 100°W-70°W as a function of latitude (Figure 2). Most models have warm SST biases north of 20°S. The magnitude of the bias varies substantially from model to model, especially around 5°S (~0-5°C). It should be noted that relatively small values of SST biases in *mri* and *cgcm* are likely to be due to the heat flux corrections (Table 1).

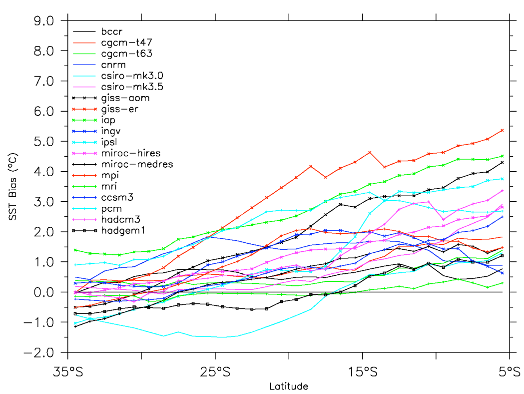

Figure 2. Biases of sea surface temperature (SST, in °C) in 19 IPCC AR4 coupled GCMs zonally averaged along 100°W-70°W as a function of latitude in the southeast Pacific Ocean. The SST biases are computed relative to World Ocean Atlas 2005 (WOA05) monthly climatology temperature data sets. The model period for computing model SST biases is January 1980 – December 1999.

4. Surface heat fluxes and upper ocean processes

Errors in both surface heat fluxes and upper ocean processes such as horizontal advection and upwelling could contribute to the warm SST biases in models. In this section, we evaluate biases in surface heat fluxes and major terms in the heat equation in models based on the comparison with those from surface flux datasets and SODA described in section 2. Since large SST biases are found mostly in the northern part of stratus region, the analysis is performed for the region north of 20°S.

4.1 Surface fluxes

a. Net surface heat fluxes

Figure 3 shows the biases of net surface heat fluxes from 17 IPCC AR4 coupled GCMs relative to the net surface heat fluxes from OAFlux (left top panel) that were averaged over the period July 1983 – December 1999. Note that two models (i.e., *ingv*, *pcm*) are not included here because surface shortwave and longwave fluxes from these models are not available. Also, note that radiation from ISCCP-FD (and thus net surface fluxes from OAFlux) is available only from 1 July 1983. The net surface heat fluxes from OAFlux are positive (warming the ocean; positive downward) in the entire region of the analysis with the magnitude ~50 – 120 W m^{-2}. All models have negative biases of net surface heat fluxes (i.e., insufficiently warming the ocean) in almost the entire region of the analysis. Positive biases are found in small regions near the coastline in some models. The nearly universal cold biases in net surface heat fluxes suggest that the warm SST biases in models are not primarily caused by errors in net surface heat fluxes.

b. Each component of surface heat flux

Biases in each component of surface heat fluxes are further examined to identify which component contributes most to negative biases of net surface heat fluxes in CGCMs. Figure 4 displays the biases (denoted by "×") of surface latent (LHF) and sensible (SHF) heat fluxes, shortwave (SW) and longwave (LW) radiation, and net surface heat fluxes averaged over the area (100°W-70°W, 20°S-5°S). The biases of these components are relative to LHF and SHF from OAFlux and SW and LW from ISCCP-FD during July 1883 – December

1999. Note that positive (negative) values in all components indicate warming (cooling) the ocean. Positive biases in SW are evident in most models, indicating too few stratus clouds over this region (e.g., Lin 2007). Thus biases in SW would contribute to warm SST biases in models. However, negative biases in LW, LHF and SHF are found in all models, and the summation of these negative biases exceeds the amount of positive biases in SW, resulting in negative biases in the net surface heat flux. The major components contributing to negative net surface heat flux biases are LHF and LW. The negative biases in LW are primarily due to too little cloud cover in models.

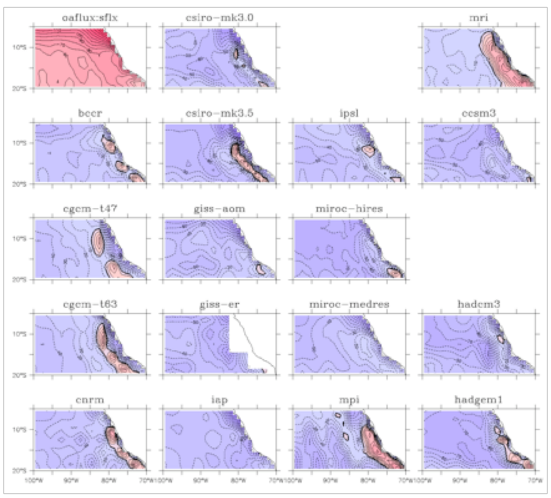

Figure 3. Top left panel: Net surface heat flux from OAFlux. Other panels: Spatial distribution of the net surface heat flux biases (shading contours in W m^{-2}) relative to OAFlux from 17 IPCC AR4 coupled GCMs in the region (100^{o}W-70^{o}W, 20^{o}S-5^{o}S) of the southeast Pacific Ocean.

Negative biases of LHF and SHF could stem from the errors of near-surface meteorological variables and SST as well as the use of different bulk flux algorithms. Figure 5 shows biases of near-surface meteorological variables averaged over the area (100^{o}W-70^{o}W, 20^{o}S-5^{o}S). The specific humidity (*qa*) is larger and wind speed (*ws*) is smaller in most models than those from OAFlux (Figs. 5a and 5d), which results in smaller *ws*(*qs*-*qa*) (Fig.5e). Hence errors in near-surface meteorological variables do not cause negative biases in LHF. Similarly, *ws*(*SST*-*Ta*) is smaller than that from OAFlux in most models (Fig. 5f) and thus errors in near-surface meteorological variables do not cause negative biases in SHF.

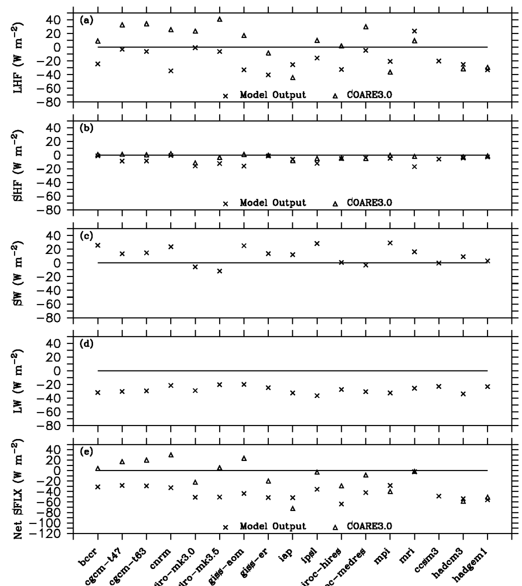

Figure 4. Biases of (a) surface latent heat flux (LHF, in W m^{-2}), (b) surface sensible heat flux (SHF, in W m^{-2}), (c) net shortwave radiation (SW, in W m^{-2}) at the ocean surface, (d) net longwave radiation (LW, in W m^{-2}) at the ocean surface, and (e) net surface heat flux (in W m^{-2}) from 17 IPCC AR4 coupled GCMs averaged in the region (100^{o}W-70^{o}W, 20^{o}S-5^{o}S). The biases are computed relative to the OAFlux monthly estimates during July 1983 – December 1999. "×" denotes the biases of heat flux directly from model output, and "Δ" denotes the biases of LHF, SHF and net surface heat flux using model variables (qa, qs, SST, ws) and the COARE bulk algorithm v 3.0.

In order to examine the impact of the use of different bulk flux algorithms on the LHF and SHF, we calculated these fluxes using the near-surface meteorological variables and SST from models along with the COARE bulk flux algorithm, which was used for the estimates of OAFlux. LHF, SHF and the net surface heat fluxes estimated with the COARE algorithm are shown in Figure 4 (indicated by "△"). Negative biases of LHF estimated with the COARE algorithm in most models are significantly reduced (less cooling of the ocean; Figure. 4a). As a result, negative biases in net surface heat fluxes are reduced in most models, indicating that surface heat flux biases are sensitive to the bulk flux algorithm.

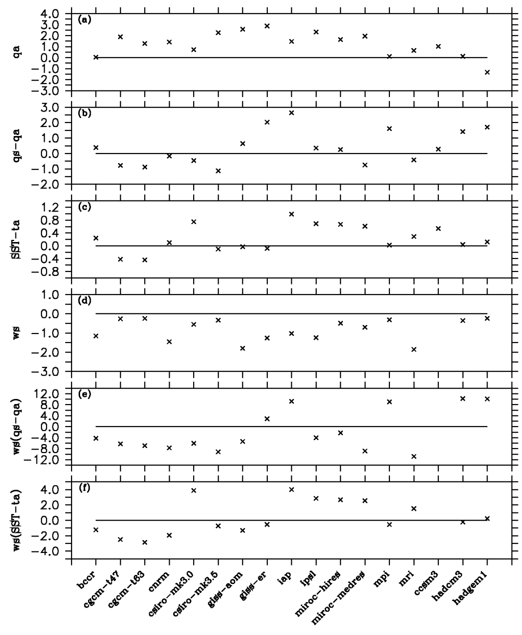

Figure 5. Biases of (a) surface air specific humidity at 2 m (qa, in g kg^{-1}), (b) difference between the saturation and air specific humidity (qs - qa, in g kg^{-1}), (c) difference between SST and air temperature at 2 m (SST – ta, in ^{o}C), (d) wind speed (ws, in m s^{-1}) at 10 m, (e) ws (qs – qa) (in m s^{-1} g kg^{-1}), and (f) ws (SST – ta) (in m s^{-1} ^{o}C) in 17 IPCC AR4 coupled GCMs area averaged in the region (100^{o}W-70^{o}W, 20^{o}S-5^{o}S). The biases are computed relative to atmospheric and oceanic variables from the OAFlux monthly estimates during July 1983 – December 1999.

c. Comparison with other surface flux datasets

Although OAFlux estimates are relatively well validated, it is difficult to determine their uncertainties because of very few in-situ observations of surface fluxes in the SEP region. In order to further confirm the negative biases in model heat fluxes, we compared model fluxes with other surface flux datasets. Net surface heat fluxes from NCEP1, NCEP2, and ERA-40 are used for the comparison. In addition to these reanalysis datasets, satellite-based latent and sensible heat fluxes (GSSTF2) and radiation (ISCCP-FD) are also used.

Figure 6 shows the biases of net surface heat flux averaged over the region (100^{o}W-70^{o}W, 20^{o}S-5^{o}S) relative to the five datasets over the period January 1988 – December 1999. While there are significant differences between the datasets, negative biases are found in all models except *MRI*, suggesting that our results on surface heat flux biases are robust at least qualitatively.

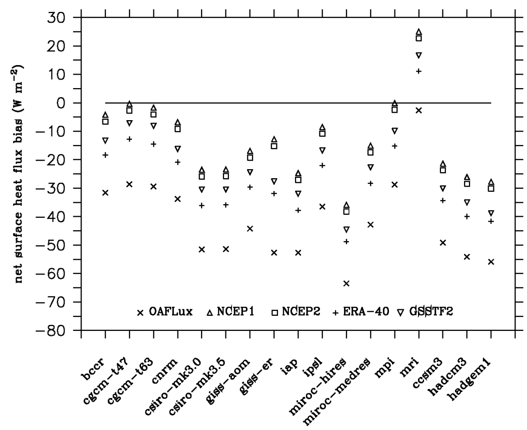

Figure 6. Biases of net surface heat flux (in W m^{-2}) in 17 IPCC AR4 coupled GCMs area averaged in the region (100^{o}W-70^{o}W, 20^{o}S-5^{o}S) relative to OAFlux (**×**), NCEP1 (△), NCEP2 (□), ERA-40 (**+**), and GSSTF2 (▽).

4.2. Upper-ocean processes

Zheng et al. (2010) indicated that three-dimensional upper ocean processes such as horizontal heat advection play an important role in controlling the annual mean SST in the stratus region based on the computation of upper ocean heat budget using OGCM experiments. Analyses similar to those in Zheng et al. (2010) are performed using the IPCC model outputs to examine the impact of errors in upper ocean processes on the SST biases.

a. Relative roles of geostrophic and Ekman heat transports

Zheng et al. (2010) examined heat transport due to both Ekman and geostrophic currents in OGCM experiments, and demonstrated that both of them significantly contribute to the upper ocean heat budget in the SEP region and that the spatial distribution of these components are notably different. Following the analysis of Zheng et al. (2010), Ekman and geostrophic heat advection in the upper 50m are computed using the output of IPCC CGCMs. Geostrophic velocities are derived from the model temperature and salinity. Ekman currents are computed as the difference between the total velocity and the geostrophic velocity (a residual from the total). It is demonstrated that Ekman currents calculated as a residual are a good approximation based on the comparison of those calculated from SODA with Ekman transports directly calculated from wind stresses (Zheng et al. 2010).

Figure 7 shows the spatial distribution of the biases in geostrophic heat advection relative to that from SODA (left top panel) over the period January 1980 – December 1999. In SODA, cold advection is evident in the open ocean and warm advection is found in the vicinity of coastal region. The positive biases of geostrophic heat advection are dominated in the open ocean in most models. Some models do not have sufficient resolutions to generate very narrow warm advection near the coast which is evident in SODA.

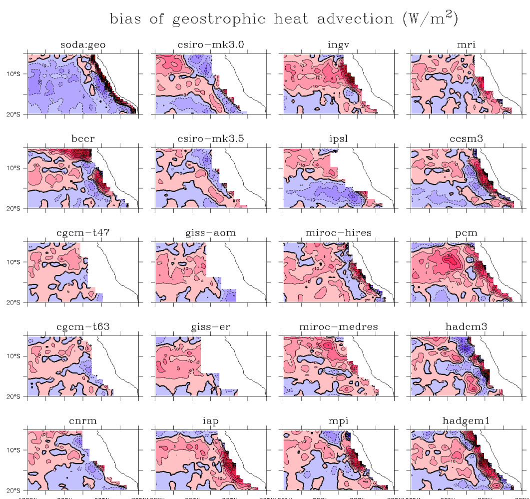

Figure 7. Top left panel: Geostrophic heat advection in the upper 50 m from SODA. Other panels: Spatial distribution of the biases in geostrophic heat advection (shading contours in W m^{-2}) in the upper 50 m from 19 IPCC AR4 coupled GCMs. The bias of model geostrophic heat advection is relative to that from SODA over the period January 1980 – December 1999.

Figure 8 shows the spatial distribution of the biases of Ekman heat advection in the upper 50 m from models relative to that in SODA (left top panel) over the period January 1980 – December 1999. In SODA, Ekman currents cause warming in the open ocean and cooling near the coast. The positive biases in Ekman heat advection are dominant in the open ocean in most models except *bccr*, *cnrm*, *ingv*, *mpi, mri, and pcm*. Similar to geostrophic heat advection, some models do not resolve large cooling near the coast which is evident in SODA.

Spatial distributions of geostrophic and Ekman heat advection from SODA (Figure 7 and 8) indicate that the sign of these terms near the coast is opposite to the open ocean. Thus processes that are responsible for the warm SST biases in the open ocean and near the coast are likely to be different. In order to identify different processes in these regions, further analyses are performed for the coastal region and open ocean separately. Figure 9 shows the biases of geostrophic and Ekman velocities and heat advection in CGCMs averaged in the entire area of the analysis (100^{o}W-70^{o}W, 20^{o}S-5^{o}S), the coastal region, and the open ocean. The coastal region is defined as the area where strong observed Ekman heat advection and coastal upwelling generally occur (5 degrees away from the coastline). The open ocean is defined as the rest of the analysis area. The average geostrophic and Ekman currents and heat advection in the coastal and open ocean areas from SODA are shown in Table 3.

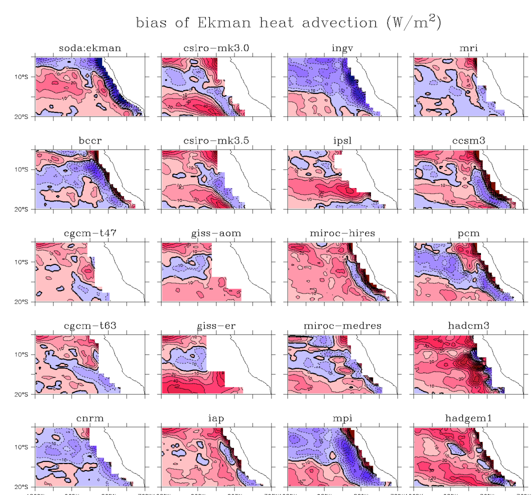

Figure 8. Same as Fig. 7, except for Ekman heat advection (in W m^{-2}).

In most models, the magnitude of biases in the area-averaged Ekman heat advection is much larger than that of geostrophic heat advection for both the coastal region and the open ocean. The area-average Ekman heat advection has relatively large positive biases (warming the ocean) both in the coastal region (ranges from 20 to 80 W m^{-2}) and open ocean (ranges from 5 to 25 W m^{-2}). Small positive biases (ranges from 0 to 10 W m^{-2}) (warming the ocean) in geostrophic heat advection are found in the open ocean for most models, while the negative biases of about -20 to -30 W m^{-2} are found in the coastal region.

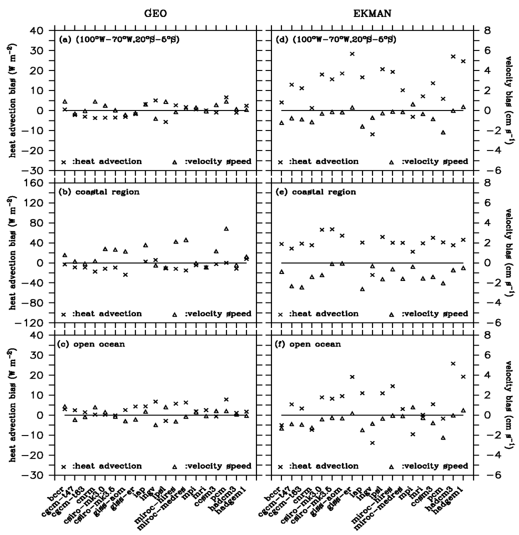

Figure 9. Biases of geostrophic heat advection (denoted by "×" in W m^{-2}) and biases of geostrophic current speed (denoted by "△" in cm s^{-1}) averaged over (a) (100°W-70°W, 20°S-5°S), (b) the coastal region between 20°S-5°S, and (c) the open ocean in the upper 50 m from 19 IPCC AR4 coupled GCMs. (d), (e), (f) Same as (a), (b), (c), except for biases of Ekman heat advection and current speed. The biases of these variables are relative to those from SODA during January 1980 – December 1999. The ordinate on the left (right) side of the panel indicates biases in heat advection (velocity). The coastal region is defined as the area 5 degrees away from the coastline.

In order to further examine how these biases are generated, geostrophic and Ekman currents and temperature of each model are described in Figure 10 and Figure 11, respectively. In the open ocean, northwestward geostrophic currents generally bring cold water near the coast to the open ocean (top left panel in Fig. 10). Most models generate similar distribution of geostrophic currents and temperature, and the biases in currents are small (Fig. 9c), resulting in the small positive biases of geostrophic heat advection in the open ocean. In the coastal region, geostrophic currents are overestimated in most models, but the negative biases in heat advection are evident (Fig. 9b) since most models do not resolve large warming due to geostrophic currents right near the coast which is evident in SODA (Fig. 7).

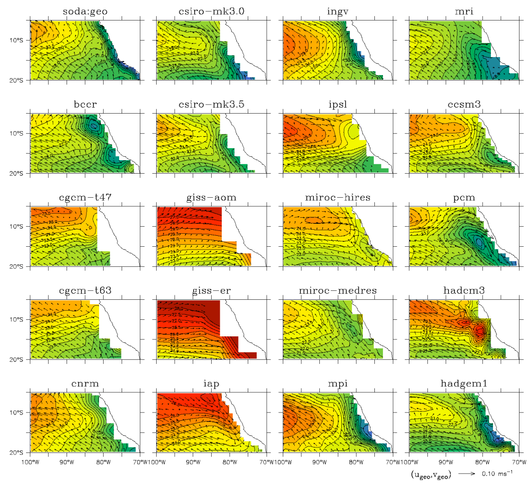

Figure 10. Geostrophic currents (arrows) and temperature (shading) in the upper 50 m from SODA (upper left panel) and IPCC AR4 CGCMs (other panels).

Southwestward Ekman currents bring warmer water at the low-latitude to higher latitude (top left panel in Fig. 11), and thus Ekman transports provide the warming in most of the area in the open ocean. Since the direction of Ekman currents is nearly parallel to the isotherms in the open ocean, the magnitude of Ekman heat advection in the upper 50 m is comparable to that of geostrophic heat advection even though the Ekman currents in this layer is much stronger (Table 3). In contrast to the relation between the direction of Ekman currents and isotherms in SODA, the isotherms in models are more zonal in the open ocean and thus the Ekman currents tend to bring warmer water to higher latitude more efficiently even though Ekman currents are relatively weaker in models (Fig. 11f). Hence, the positive (warm) biases in Ekman heat advection are generated in the open ocean. In the coastal region, Ekman currents cause cooling because they bring the cold upwelled water to the offshore direction (top left panel in Fig. 11). Since Ekman currents in the coastal region are underestimated in most models (Fig. 9e) and large cooling of Ekman transport (which is evident in SODA) is not well resolved in most models (Fig. 8), the cooling due to the advection is reduced, resulting in the positive biases of Ekman heat advection.

b. Vertical heat advection and coastal upwelling

Figure 12c and 12f show the vertical advection term defined as $-\rho C_p wdT/dz$ (in W m^{-3}) at 50 m for the coastal region and the open ocean. While no systematic bias of this term is found in the coastal region, the significant cold biases are evident in the open ocean. The underestimate of downward velocity in the open ocean in models is mostly responsible for the cold biases. In the coastal region, the upwelling is overly weak in most models. However, because of the overly large temperature gradient in some models, systematic biases are not clearly found. Also, it is not clear whether vertical heat advection at 50 m significantly affects SSTs in the coastal region since it may strongly depend on the temperature profile above 50 m.

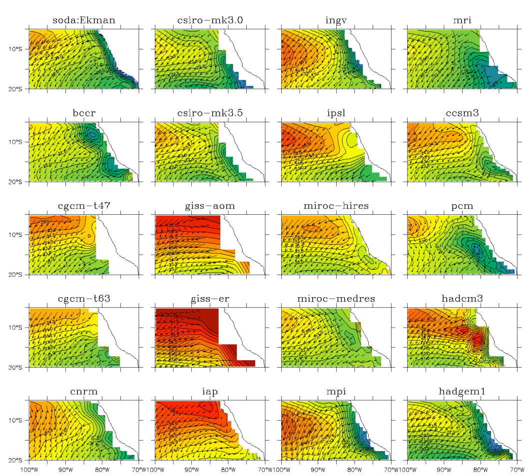

Figure 11. Same as in Fig. 10, except for Ekman currents.

In order to further examine the influence of vertical heat advection on SSTs, the circulation and temperature in the zonal-vertical plane are described. Figure 15 shows the zonal circulation and temperature along 15^{o}S averaged over January 1980 – December 1999 from SODA and CGCMs. Strong coastal upwelling occurs within 3-5 degrees away from the coast in SODA. The cold upwelled water is then transported away from the coast by the mean currents. The coastal upwelling is underestimated in most models, and temperature profiles near the coast suggest that cold subsurface water affects SSTs less than those in SODA. This is further demonstrated in the depth of 18^{o}C isotherm along 15^{o}S (Fig. 14). While 18^{o}C isotherms are shallower in most models than those in SODA west of 78W, the upwelling is not strong enough to bring water colder than 18^{o}C to the surface at the coast. This indicates that upwelling in most models is weaker and broader than that in SODA. The broader upwelling can influence SST in the open ocean through vertical heat advection, but the magnitude is much smaller than horizontal heat advection (Fig. 9 and Fig. 12). It should be noted that similar results are found at other latitudes between 10^{o}S and 20^{o}S.

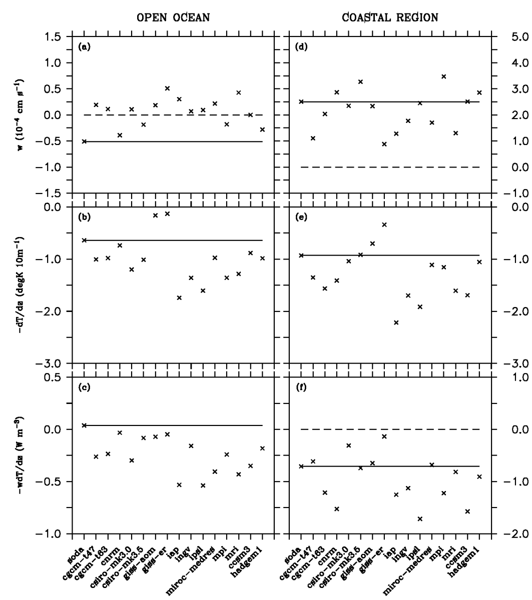

Figure 12. (a) Vertical velocity (*w,* in 10^{-4} cm s^{-1}) at 50 m depth, (b) $-dT/dz$ (in degK 10m^{-1}) at 50 m depth, and (c) $-\rho C_p wdT/dz$ (in W m^{-3}) at 50 m averaged in the open ocean area from SODA and 15 IPCC AR4 coupled GCMs. (d), (e), (f) Same as (a), (b), (c), except for those averaged in the coastal region.

The broad and weak upwelling could be due to a combination of coarse horizontal resolution of ocean models (Table 1) and underestimates of alongshore winds. Figure 15 shows the strength of alongshore wind stress in CGCMs compared to that in SODA. All models have weaker alongshore wind stresses at most latitudes. Hence the relation between biases in upwelling and alongshore winds is consistent. However, it is difficult to identify the ultimate sources of these biases since a variety of processes in the atmosphere and ocean as well as air-sea feedback are involved in determining them in CGCMs.

5. Discussion

This study focuses on identifying the errors of upper ocean processes and air-sea fluxes in CGCMs that could contribute to SST biases in the SEP region. It is worth reemphasizing that the net causes of these SST biases are likely ultimately determined by a combination of atmospheric, land, and oceanic processes, along with air-sea feedback processes that could amplify the errors in both AGCM and OGCM components. For example, strong alongshore winds at the coasts of Chile and Peru are primarily caused by the great height of the Andes Cordillera that acts as a barrier to zonal flow in the South Pacific (Garreaud and Muñoz 2005). In fact, a recent CGCM study (Gent et al. 2009) demonstrated that a high-resolution AGCM that can better resolve the orography of the Andes Cordillera allows strongest surface winds in the upwelling region to be located much closer to the coasts, which generate stronger coastal upwelling, resulting in reduced SSTs. The colder SST and near-surface air temperature generate more stratus clouds, which shield the sunlight reaching the ocean, and further reduce the SST. Further studies that focus on atmospheric, land, and air-sea feedback processes are necessary to precisely identify the combination of sources of SST biases in CGCMs in this region.

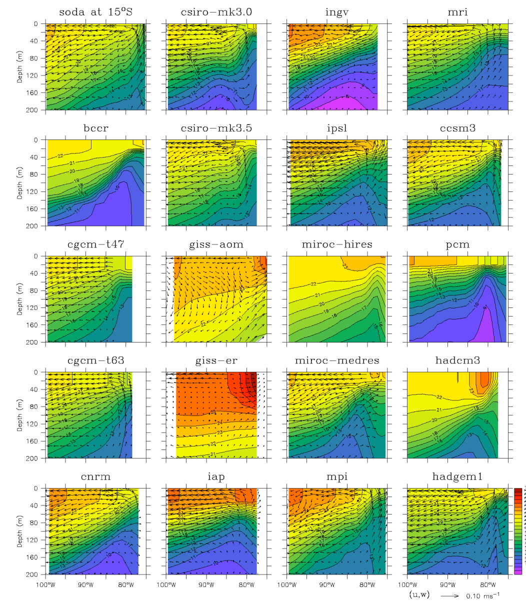

Figure 13. Circulation (vectors in m s^{-1}) and temperatures (shading contours in ^{o}C) in the zonal-vertical plane at 15^{o}S averaged over January 1980 – December 1999 from SODA (upper left panel) and 19 IPCC AR4 coupled GCMs. Contour interval is 1 ^{o}C.

Since none of the IPCC AR4 coupled GCMs resolve mesoscale and submesoscale eddies because of the coarse horizontal resolution, the role of eddy activity in the warm SST biases could not be investigated in this study. Recent independent high-resolution modeling studies (Zheng et al. 2010; Toniazzo et al. 2010) indicated that long-term mean area-averaged eddy heat flux divergence is small over the SEP region. Thus resolving mesoscale and submesoscale eddies in CGCMs may not necessarily reduce SST biases in this region.

In this study, OAFlux and SODA are primarily used to determine CGCMs' errors in surface heat fluxes and upper ocean currents and temperatures. While these datasets are useful for evaluating current CGCMs that include substantial errors in surface fluxes and upper ocean variables in the SEP region, there could be significant uncertainties in these analyses. However, it is difficult to validate these datasets since there were few in-situ measurements of upper ocean and surface fluxes in the SEP region until recently. Intensive in-situ observations of upper ocean and atmospheric boundary layer including air-sea fluxes were conducted in fall 2008 as part of VAMOS Ocean-Cloud-Atmosphere-Land Study (VOCALS; Wood et al. 2007). A substantial amount of data collected during the VOCALS Regional Experiment (REx) would be useful to evaluate a variety of surface flux datasets and ocean analysis and to validate various schemes used in the analysis such as the bulk flux algorithm. Hopefully, these global datasets will be further improved after the validation and evaluation of the analyses based on the comparison with the data from VOCALS REx as well as other observations.

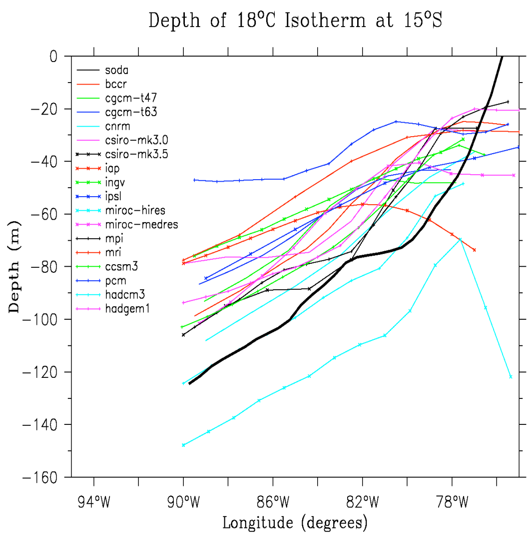

Figure 14. Depth of 18^{o}C isotherm along 15^{o}S averaged over the period January 1980 – December 1999 from SODA and 17 IPCC AR4 coupled GCMs. Two models (giss-anom and giss-er) are excluded because of their extreme values (see also Fig. 13).

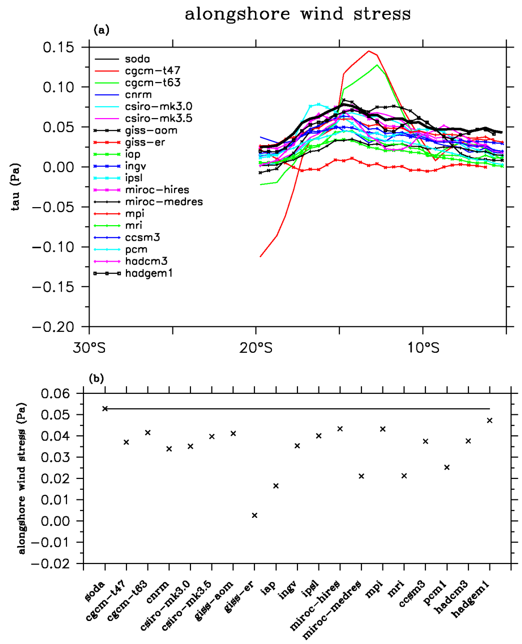

Figure 15. (a) Alongshore wind stress (in Pa) as a function of latitude, and (b) alongshore wind stress averaged in latitude (20^{o}S-5^{o}S) over the period January 1980 – December 1999 from SODA and 18 IPCC AR4 coupled GCMs.

The analysis of the upper ocean shows that most CGCMs underestimate coastal upwelling. While the alongshore winds in the AGCMs are weaker than observed and partially responsible for the weaker upwelling, the horizontal resolution in the OGCMs is not adequate to resolve strong and narrow upwelling. Accordingly, improving the horizontal resolution in the OGCM component may reduce warm SST biases in the coastal region. Also, if more cold water is upwelled at the coast, warm SST biases in the open ocean could be reduced by horizontal advection of this water from the coast.

The result also shows that cold water (less than 18^{o}C) is upwelled to around 30-40 m depth in many models (Fig. 13, Fig.14) but this does not significantly affect SST in most models possibly because mixing in the upper layer is not sufficiently strong. While the improvement of mixing schemes is a major challenge in ocean modeling, this might also improve SST biases in some models. Further studies that focus on the improvement of upper-ocean mixing parameterization are certainly desirable. For example, OGCM and one dimensional ocean model experiments could be performed to examine the sensitivity of the upper ocean temperature and SST near the coast to different mixing schemes. Comparisons with high quality and fine resolution data in the upper ocean obtained during VOCALS REx would be very useful for such studies.

The underestimated alongshore winds in the AGCM component of IPCC AR4 models could partly be attributed to overestimated precipitation in the SEP region (Davis et al. 2010, manuscript in preparation). Although deep convection is rarely observed in the SEP region, many IPCC AR4 models produce substantial precipitation in this region, which is associated with the double inter-tropical convergence zone (ITCZ) problem (Lin 2007). The excess precipitation lowers the sea level pressure because the release of latent heat due to unrealistically high precipitation heats up and expands the atmosphere locally. Thus, the subtropical high is weakened, leading to weaker alongshore winds. Lin (2007) hypothesized that the overestimation of tropical precipitation in IPCC AR4 models is caused by their lack of the observed self-suppression processes in tropical convection, such as the sensitivity of convective updrafts to lower troposphere moisture, the cooling and drying of boundary layer by convective downdrafts, and the warming and drying of lower troposphere by mesoscale downdrafts. Including these processes into the model deep convection schemes may help lead to a more realistic upper ocean state by reducing the excessive precipitation in the SEP region and enhancing the subtropical high and alongshore winds.

6. Summary

This study investigates processes in the upper ocean and air-sea fluxes that could contribute to systematic SST biases under stratus cloud decks in the southeast Pacific in 19 IPCC AR4 coupled GCMs. Surface fluxes and upper ocean variables from the output of CGCMs are analyzed, and they are compared with surface flux estimates (OAFlux) and the ocean analysis (SODA) derived from a variety of satellite measurements and reanalyses. Nearly universal warm SST biases in CGCMs are found, and the biases are larger in the northern part of stratus region especially north of 20^{o}S.

In contrast to warm SST biases, negative biases (cooling the ocean) in net surface heat flux are found in most CGCMs, indicating that errors in surface heat fluxes do not significantly contribute to their SST biases. The negative biases in latent heat flux and longwave radiation are mostly responsible for the negative net surface heat flux biases. Positive biases in shortwave radiation are found in most models because they do not generate sufficient stratus clouds. The use of varying bulk flux algorithms is found to be partially responsible for the negative biases of latent heat flux based on the flux estimates using the COARE algorithm, near-surface meteorological variables and SST from the model output.

Since horizontal heat advection strongly influence the annual mean heat budget (and thus SST) (Colbo and Weller 2007, Zheng et al. 2010), heat advection due to geostrophic and Ekman currents are estimated using the CGCM outputs. Our results suggest that positive biases in errors of Ekman heat advection primarily contribute to the warm SST biases, while the contribution of the errors in geostrophic heat advection is still significant. Near the coast of Peru and Chile, the warm SST biases are attributed to the weaker Ekman currents that transport less cold upwelled water at the coast offshore. In the open ocean, southwestward Ekman currents bring warm water near the equator southward more efficiently because the isotherms in CGCMs are more zonal than in observations.

Most CGCMs underestimate alongshore winds and coastal upwelling, which contributes to the warm SST biases both in the offshore and coastal regions. Upwelling in most CGCMs is weaker and broader than observations. It is suggested that the coarse resolution of OGCM component is partially responsible for the weak and broad upwelling in CGCMs. Therefore, we hypothesize here that the improvement of horizontal resolution in OGCM components of CGCMs will reduce the warm SST biases in the SEP region. Improvement in resolution and in convection schemes in AGCM component of CGCMs could also help better simulate alongshore winds, thus leading to a more realistic upper ocean state.

REFERENCES

Antonov, J. I., R. A. Locarnini, T. P. Boyer, A. V. Mishonov, and H. E. Garcia, 2006. World Ocean Atlas 2005, Volume 2: Salinity. S. Levitus, Ed. NOAA Atlas NESDIS 62, U.S. Government Printing Office, Washington, D.C., 182 pp.

Brunke, M. A., C. W. Fairall, X. Zeng, L. Eymard, and J. A. Curry, 2003: Which bulk aerodynamic algorithms are least problematic in computing ocean surface turbulent fluxes? *J. Climate*, **16**, 619-635.

Carton, J. A., and B. S. Giese, 2008: A reanalysis of ocean climate using Simple Ocean Data Assimilation (SODA). *Mon. Wea. Rev*., **136**, 2999-3017.

Carton, J. A., G. A. Chepurin, X. Cao, and B. S. Giese, 2000a: A Simple Ocean Data Assimilation analysis of the global upper ocean 1950-1995, Part 1: methodology. *J. Phys. Oceanogr.*, **30**, 294-309.

Carton, J. A., G. A. Chepurin, and X. Cao, 2000b: A Simple Ocean Data Assimilation analysis of the global upper ocean 1950-1995, Part 2: results. *J. Phys. Oceanogr.*, **30**, 311-326.

Chaigneau, A., and O. Pizarro, 2005a: Mean surface circulation and mesoscale turbulent flow characteristics in the eastern South Pacific from satellite tracked drifters. *J. Geophys. Res*., **110**, doi: 10.1029/2004JC002628

Chaigneau, A., and O. Pizarro, 2005b: Eddy characteristics in the eastern South Pacific. *J. Geophys. Res*., **110**, doi: 10.1029/2004JC002815.

Chou, S.-H., E. Nelkin, J. Ardizzone, R. M. Atlas, and C.-L. Shie, 2003:Surface turbulent heat and momentum fluxes over global oceans based on the Goddard satellite retrievals, version 2 (GSSTF2). *J. Climate*, **16**, 3256-3273.

Chou, S.-H., E. Nelkin, J. Ardizzone, and R. M. Atlas, 2004: A comparison of latent heat fluxes over global oceans for four flux products. *J. Climate*, **17**, 3973-3989.

Colbo, K, and R. Weller, 2007: The variability and heat budget of the upper ocean under the Chile-Peru stratus. *J. Mar. Res*., **65**, 607-637.

Davis, M., J. L. Lin, T. Qian, and M.-P. Hung, 2010: Ocean-atmosphere feedback in the southeastern Pacific simulated by 24 IPCC AR4 coupled GCMs. (in preparation).

de Szoeke, S. P., and X.-P. Xie, 2008: The tropical eastern Pacific seasonal cycle: assessment of errors and mechanisms in IPCC AR4 coupled ocean-atmosphere general circulation models. *J. Climate*, **21**, 2573-2590.

Fairall, C. W., E. F. Bradley, J. E. Hare, A. A. Grachev, and J. B. Edson, 2003: Bulk parameterization of air-sea fluxes: updates and verification for the COARE algorithm. *J. Climate*, **16**, 571-591.

Garreaud, R. D., and R. C. Muñoz, 2005: The Low-Level Jet off the West Coast of Subtropical South America: Structure and Variability. Monthly Weather Review: 133, 2246–2261.

Gent, P. R., S. G. Yeager, R. B. Neale, S. Levis, and D. A. Bailey, 2009: Improvements in a half degree atmosphere/land version of the CCSM. *Climate Dyn*., **79**, 25-58, doi: 10.1007/s00382-009-0614-8.

Gordon, C. T., A. Rosati, and R. Gudgel, 2000: Tropical sensitivity of a coupled model to specified ISCCP low clouds. *J. Climate*, **13**, 2239-2260.

Hormazabal, S., G. Shaffer, and O. Leth, 2004: Coastal transition zone off Chile. *J. Geophys. Res.*, **109**, C01021, doi: 10.1029/2003JC001956.

Jones, P. W., 1999: First- and second-order conservative remapping schemes for grids in spherical coordinates. *Mon. Wea. Rev*., **127**, 2204-2210.

Kalnay et al., 1996: The NCEP/NCAR 40-year reanalysis project. *Bull. Amer. Meteor. Soc.*, 77, 437-470.

Kanamitsu, M., W. Ebisuzaki, J. Woolen, J. Potter, and M. Fiorino, 2002: NCEP/DOE AMIP-II Reanalysis (R-2). *Bull. Amer. Met. Soc*., **83**, 1631-1643.

Kiehl, J. T., and P. R. Gent, 2004: The Community Climate System Model, version 2, *J. Climate*, 17, 3666-3682.

Klein, S. A., D. L. Hartmann, and J. R. Norris, 1995: On the relationship among low cloud structure, sea surface temperature, and atmospheric circulation in the summertime northeast Pacific. *J. Climate*, **8**, 1140-1155.

Kubota, M., A. Kano, H. Muramatsu, and H. Tomita, 2003: Intercomparison of various surface heat flux fields. *J. Climate*, **16**, 670-678.

Large, W. G., and G. Danabasoglu, 2006: Attribution and impacts of upper-ocean biases in CCSM3. *J. Climate*, **19**, 2325-2346.

Large, W. G., J. C. McWilliams, and S. C. Doney, 1994: Oceanic vertical mixing: Review and model with a nonlocal boundary layer parameterization. *Rev. Geophys*., **32**, 363-403.

Lin, J. L., 2007: The double-ITCZ problem in IPCC AR4 coupled GCMs: Ocean-atmosphere feedback analysis. *J. Climate*, **20**, 4497-4525.

Locarnini, R. A., A. V. Mishonov, J. I. Antonov, T. P. Boyer, and H. E. Garcia, 2006. World Ocean Atlas 2005, Volume 1: Temperature. S. Levitus, Ed. NOAA Atlas NESDIS 61, U.S. Government Printing Office, Washington, D.C., 182 pp.

Ma, C.-C., C. R. Mechoso, A. W. Robertson, and A. Arakawa, 1996: Peruvian stratus clouds and the tropical Pacific circulation: A coupled ocean-atmosphere GCM study. *J. Climate*, **9**, 1635-1645.

McAvaney, B., and Coauthors, 2001: Model evaluation. *Climate Change 2001: The Scientific Basis*, J. T. Houghton et al., Eds., Cambridge University Press, 471-523.

Mechoso, C. R., and coauthors, 1995: The seasonal cycle over the tropical Pacific in coupled ocean-atmosphere general circulation models. *Mon. Wea. Rev*., **123**, 2825-2838.

Miller, R. L., 1997: Tropical thermostats and low cloud cover. *J. Climate*, **10**, 409-440.

Norris, J. R., and C. B. Leovy, 1994: Interannual variability in stratiform cloudiness and sea surface temperature. *J. Climate*, **7**, 1915-1925.

Rossow, W. B., A. W. Walker, D. E. Beuschel, and M. D. Roiter, 1996: International Satellite Cloud Climatology Project (ISCCP) documentation of new cloud datasets. WMO Tech. Doc. 737, 115pp.

Penven, P., V. Echevin, J. Pasapera, F. Colas, and J. Tam, 2005: Average circulation, seasonal cycle, and mesoscale dynamics of the Peru Current System: a modeling approach. *J. Geophys. Res*., **110**, doi: 10.1029/2005JC002945.

Schubert, W. H., 1976: Experiments with Lilly's cloud-topped model. *J. Atmos. Sci*., **33**, 436-446.

Shinoda, T., and J. L. Lin, 2009: Interannual variability of the upper ocean in the southeast Pacific stratus cloud region. *J. Climate*, **22**, 5072-5088.

Simmons, A. J., and J. K. Gibson, 2002: The ERA-40 Projects Plan, Series #1, ECMWF, Shinfield Park, Reading, UK, 63pp.

Smith, R. D., J. K. Dukowicz, and R. C. Malone, 1992: Parallel ocean general circulation modeling. *Physica D*., **60**, 38-61.

Toniazzo, T., C. R. Mechoso, L. C. Shaffrey, and J. M. Slingo, 2010: Upper-ocean heat budget and ocean eddy transport in the south-east Pacific in a high-resolution coupled model. Clim. Dyn., doi: 10.1007/s00382-009-0703-8.

Uppala, S. M., and co-authors, 2005: The ERA-40 re-analysis. *Quart. J. R. Meteorol. Soc.*, **131**, 2961-3012. doi:10.1256/qj.04.176.

Wittenberg, A. T., A. Rosati, N-C. Lau, and J. J. Ploshay, 2006: GFDL's CM2 Global Coupled Climate Models. Part III: Tropical Pacific climate and ENSO. *J. Climate*, **19**, 698-722.

Wood, R., C. Bretherton, B. Huebert, C. R. Mechoso, and R. Weller, 2007: The VAMOS Ocean-Cloud-Atmosphere-Land Study (VOCALS): Improving understanding, model simulations, and prediction of the southeast Pacific climate system. Post-VOCALS-Rex Rep. [Available online at http://www.eol.ucar.edu/projects/vocals/.]

Xie, S.-P., 2004: The shape of continents, air-sea interaction, and the rising branch of the Hadley circulation. *The Hadley Circulation: Past, Present and Future*, H. F. Diaz and R. S. Bradley, Eds., Kluwer Academic Publishers, Dordrecht, 121-152.

Yu, L., and R. A. Weller, 2007: Objectively analyzed air-sea fluxes for the global ice-free oceans (1981-2005). *Bull. Amer. Meteor. Soc.*, **88**, 527-539.

Yu, L., X. Jin, and R. A. Weller, 2008: Multidecade global flux datasets from the objectively analyzed air-sea fluxes (OAFlux) Project: Latent and sensible heat fluxes, ocean evaporation, and related surface meteorological variables. Woods Hole Oceanographic Institution, OAFlux Project Tech. Rep., OA-2008-01, 64pp.

Zhang Y.-C., W. B. Rossow, A. A. Lacis, V. Oinas, and M. I. Mishchenko, 2004: Calculation of radiative fluxes from the surface to top of atmosphere based on ISCCP and other global data sets: Refinements of the radiative transfer model and the input data. J. Geophys. Res., 109, D19105, doi:10.1029/2003JD004457.

Zheng, Y., and B. S. Giese, 2009: Ocean heat transport in Simple Ocean Data Assimilation: structure and mechanisms. *J. Geophys. Res.*, **114**, C11009, doi: 10.1029/2008JC005190.

Zheng, Y., T. Shinoda, G. N. Kiladis, J.-L. Lin, E. J. Metzger, H. E. Hurlburt, and B. S. Giese, 2010: Upper-ocean processes under the stratus cloud deck in the southeast Pacific Ocean. *J. Phys. Oceanogr.*, **40**, 103-120.

Table lists:

Table 3. Magnitude of geostrophic, Ekman velocity and the resultant heat advection from SODA averaged in the area (100°W-70°W, 20°S-5°S), the coastal region, and the open ocean over the period January 1980 – December 1999. Units: cm s^{-1} for velocity, and W m^{-2} for heat advection.

SODA	V_{geo}	V_{ek}	H_{geo}	H_{ek}
(100°W-70°W, 20°S-5°S)	2.95	4.86	-6	-3
Coastal region	2.28	4.31	14	-38
Open ocean	3.12	5.00	-11	6

Table 2. List of monthly observational datasets used in this study.

Variables	Dataset	Spatial coverage/resolution (degrees)	Temporal coverage	Reference
Ocean temperature and salinity	SODA WOA05	Global ocean 0.5x0.5-L40 Global ocean 1x1-L24	Jan1958 - Dec 2005 Monthly Climatology	Carton and Giese (2008) Locarnini et al. (2006) Antonov et al. (2006)
Ocean velocity	SODA	Global ocean 0.5x0.5-L40	Jan1958 - Dec 2005	Carton and Giese (2008)
Surface wind stress	ERA-40	Global ocean 0.5x0.5	Jan1958 - Dec 2001	Simmons and Gibson (2002)
Net surface heat flux	OAFlux NCEP1 NCEP2 ERA-40	Global ocean 1x1 Global ocean 1.9x1.9 Global ocean 1.9x1.9 Global ocean 2.5x2.5	July 1983 - Dec 2007 Jan 1948 - present Jan 1979 - Dec 2008 Sep 1957 - Aug 2002	Yu and Weller (2007) Kalnay et al. (1996) Kanamitsu et al. (2002) Uppala et al. (2005)
Surface latent/sensible heat flux	OAFlux GSSTF2	Global ocean 1x1 Global ocean 1x1	Jan 1958 - Dec 2008 Jan 1988 - Dec 2000	Yu and Weller (2007) Chou et al. (2003)
Net surface shortwave /longwave flux	ISCCP-FD	Global ocean 1x1	July 1983 - Dec 2007	Rossow et al. (1996) Yu and Weller (2007)
Air temperature at 2 m	OAFlux	Global ocean 1x1	Jan 1958 - Dec 2008	Yu and Weller (2007)
Sea surface skin temperature	OAFlux	Global ocean 1x1	Jan 1958 - Dec 2008	Yu and Weller (2007)
Air specific humidity at 2 m	OAFlux	Global ocean 1x1	Jan 1958 - Dec 2008	Yu and Weller (2007)
Wind speed at 10 m	OAFlux	Global ocean 1x1	Jan 1958 - Dec 2008	Yu and Weller (2007)

SODA: Simple Ocean Data Assimilation.
WOA05: World Ocean Atlas 2005.
NCEP: National Center for Environmental Prediction
ERA-40: 40-yr ECMWFRe-Analysis.
OAFlux: Objectively Analyzed air-sea heat Fluxes.
GSSTF2: Goddard Satellite-Based Surface Turbulent Fluxes Version 2.
ISCCP-FD: International Satellite Cloud Climatology Project Flux Datasets.

Table 1. List of 19 IPCC AR4 coupled GCMs that participate in this study.

Modeling Groups	IPCC ID (label in figures)	Resolution[a] (degrees)[b]	Heat flux correction	Run #
Bjerknes Centre for Climate Research	BCCR-BCM2.0 (bccr)	360x180-L33 (1x1)	None	1
Canadian Centre for Climate Modeling and Analysis	CGCMA3.1-T47 (cgcm-t47)	192x96-L29 (1.9x1.9)	Yes	1
Canadian Centre for Climate Modeling and Analysis	CGCMA3.1-T63 (cgcm-t63)	256x192-L29 (1.4x0.93)	Yes	1
Météo-France / Centre National de Recherches Météorologique	CNRM-CM3 (cnrm)	180x170-L33 (2x1)	None	1
CSIRO Atmospheric Research	CSIRO-Mk3.0 (csiro-mk3.0)	192x189-L31 (1.9x0.93)	None	2
CSIRO Atmospheric Research	CSIRO-Mk3.5 (csiro-mk3.5)	192x189-L31 (1.9x0.93)	None	1
NASA / Goddard Institute for Space Studies	GISS-AOM (giss-aom)	90x60-L31(4x3)	None	1
NASA / Goddard Institute for Space Studies	GISS-ER (giss-er)	72x46-L33 (5x4)	None	1
LASG / Institute of Atmospheric Physics	FGOALS-g1.0 (iap)	360x170-L33 (1x1)	None	1
Instituto Nazionale di Geofisica e Vulcanologia	INGV-SXG (ingv)	360x180-L33 (1x1)	None	1
Institut Pierre Simon Laplace	IPSL-CM4 (ipsl)	180x170-L31(2x1)	None	1
Center for Climate System Research (The University of Tokyo), National Institute for Environmental Studies, and Frontier Research Center for Global Change	MIROC3.2-hires (miroc-hires)	320x320-L33 (1.1x0.56)	None	1
Same as above	MIROC3.2-medres (miroc-medres)	256x192-L33 (1.4x0.93)	None	2
Max Planck Institute for Meteorology	ECHAM5/MPI-OM (mpi)	360x180-L40 (1x1)	None	1
Meteorological Research Institute	MRI-CGCM2.3.2 (mri)	144x111-L23 (2.5x2)	Yes[c]	1
National Center for Atmospheric Research	CCSM3 (ccsm3)	320x395-L40 (1.1x0.27)[d]	None	1
National Center for Atmospheric Research	PCM (pcm)	360x180-L32 (1x1)	None	3
Hadley Centre for Climate Prediction and Research / Met Office	UKMO-HadCM3 (hadcm3)	288x144-L20 (1.25x1.25)	None	1
Hadley Centre for Climate Prediction and Research / Met Office	UKMO-HadGEM1 (hadgem1)	360x216-L40 (1x0.7)[d]	None	1

[a]Resolution is about ocean model output which is denoted by grid points in longitude x latitude and # of vertical layers.
[b]Parenthesis shows horizontal resolution (longitude x latitude) in degrees around the stratus region (100°W-70°W, 35°S-5°S).
[c]Monthly climatological flux adjustment for heat (only 12°S-12°N) is used.
[d]Grid points are not even in latitude, resolution in latitude is finer as it gets closer to the equator.